



In silico investigations on the binding efficacy and allosteric mechanism of six different natural product compounds towards PTP1B inhibition through docking and molecular dynamics simulations

Baskaran SarathKumar¹ · Baddireddi Subhadra Lakshmi¹

Received: 2 February 2019 / Accepted: 16 August 2019 / Published online: 26 August 2019
© Springer-Verlag GmbH Germany, part of Springer Nature 2019

Abstract

Protein tyrosine phosphatase 1B (PTP1B) is a major negative regulator of both the insulin and leptin receptor phosphorylation which impacts insulin sensitivity and hence is a major therapeutic target for the treatment of type 2 diabetes and obesity. Identification of PTP1B active site inhibitors has proven to be difficult with none of them clearing the phase II clinical trials. Since the conventional methods of targeting the active site of PTP1B have failed to bring out effective PTP1B inhibitors as potential drugs, recent studies are focussing on identification of potential allosteric inhibitors of PTP1B with better specificity and activity. A complete understanding of the molecular features dynamically involved for allosteric site inhibition is still uncertain, and hence, this study is aimed at evaluating the allosteric effectiveness of six natural compounds isolated from medicinal plants which showed in vitro antidiabetic activity along with PTP1B inhibition. The allosteric binding and inhibition of these compounds are studied using computational methods such as molecular docking, homology modelling and molecular dynamics simulations for a timescale of 100 ns. The molecular dynamics simulations of native PTP1B, along with the modelled allosteric α -7 helix, for a timescale of 100 ns, revealed the spontaneous transition of the native PTP1B from open WPD loop (active) to closed WPD loop (inactive) conformations during the simulations. Similar dynamics was observed in the presence of the active site substrate pTyr (phosphotyrosine), whereas this transition was inhibited in the presence of the compounds at the allosteric site. Results of molecular dynamics simulations and principal component analysis reveal that the hindrance to WPD loop was mediated through structural interactions between the allosteric α -helical triad with Loop11 and WPD loop. The MM-PBSA (Molecular Mechanics - Poisson Boltzmann with Surface Area solvation) binding energy results along with H-bonding analysis show the possible allosteric inhibition of Aloe emodin glycoside (AEG), 3 β -taraxerol (3BT), chlorogenic acid (CGA) and cichoric acid (CHA) to be higher in comparison with (3 β)-stigmast-5-en-3-ol (SGS) and methyl lignocerate (MLG). The interaction analysis was further validated by scoring the allosteric complexes before and after MD simulations using Glide. These findings on spontaneous PTP1B fluctuations and the allosteric interactions provide a better insight into the role of PTP1B fluctuations in impacting the binding energy of allosteric inhibitors towards optimal drug designing for PTP1B.

Keywords Molecular docking · Homology modelling · Molecular dynamics simulation · PTP1B allosteric inhibitors · PCA · MM-PBSA analysis · Glide docking · Binding energy analysis · Allosteric α -7 helix

Electronic supplementary material The online version of this article (<https://doi.org/10.1007/s00894-019-4172-7>) contains supplementary material, which is available to authorized users.

✉ Baddireddi Subhadra Lakshmi
lakshmi@annauniv.edu; lakshmi1@gmail.com

¹ Department of Biotechnology, Anna University, Chennai, Tamil Nadu 600 025, India

Introduction

Protein tyrosine phosphatases (PTPs) are an important group of enzymes among the phosphatase family involved in multifactorial metabolic pathways. Among them, PTP1B plays a major role in metabolic disorders like type 2 diabetes and obesity by acting as a dephosphorylating agent in insulin and leptin signalling pathways. Knockout mice lacking PTP1B have been reported

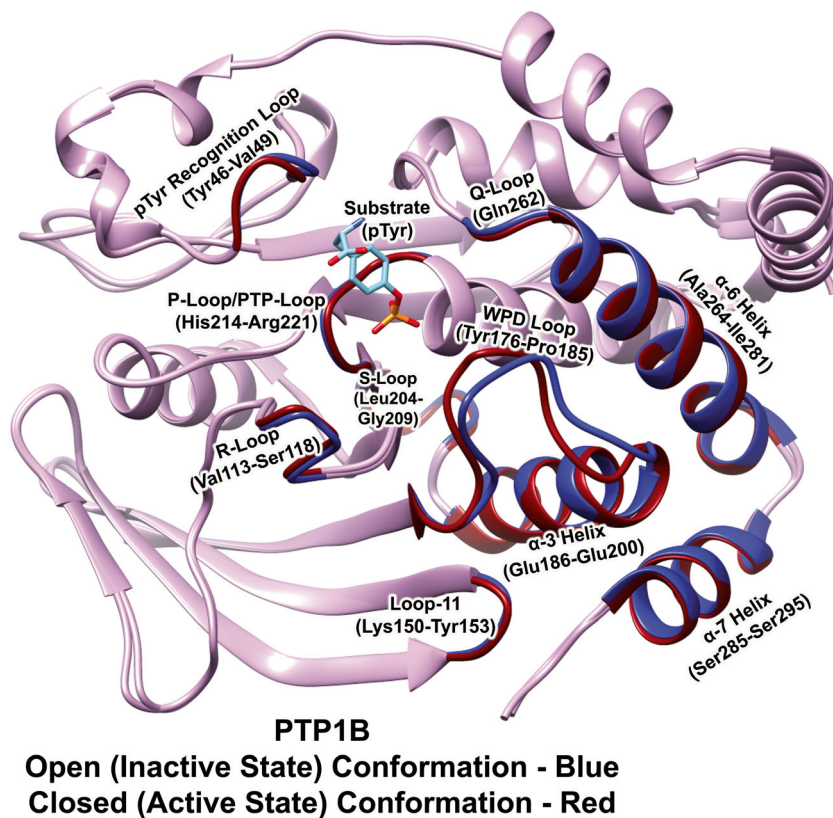
to be highly sensitive to insulin action and resistant to diet-induced obesity [1, 2].

PTP1B has a signature motif, (I/V)HCXAGXXR(S/T)G, at the catalytic active site along with the catalytic WPD loop, characteristically conserved with other PTPs from bacteria to mammals and a 72% homologue identity towards T cell protein tyrosine phosphatases (TC-PTP) [3, 4]. Hence, it has been a great challenge for the identification and development of potential drug compounds as PTP1B inhibitors for optimal treatment of insulin resistance and obesity [5, 6]. The canonical structure of PTP1B consists of 435 amino acids with a molecular weight of ~45 kDa. Though there are more than 200 solved crystallographic structures along with co-crystal complexes available in the Protein Data Bank, due to the disordered loop at the C-terminal, most of the deposited PTP1B crystallographic structures contain only the active protein fragment consisting of 299 amino acid residues. Studies have shown the activity of PTP1B to be based on the conformational mechanism of the catalytic WPD loop (Tyr176-Pro185) [7]. The PTP1B protein stays in an apo-inactive state with catalytic WPD loop in an open conformation making the active site accessible to the substrate. Upon binding of the substrate, the protein undergoes conformational changes to active state by enabling the WPD loop to closed conformation [4]. In addition, there are other domain regions involved in the activation [8–10] and assisting the conformational changes of WPD loop (Tyr176-Pro185), which include the R loop

(Val113-Ser118), P loop/PTP loop (His214-Arg221), pTyr recognition loop (Tyr46-Val49), Q loop (Gln262), S loop (Leu204-Gly209), Loop11 (Lys150-Tyr153), α -3 helix (Glu186-Glu200), α -6 helix (Ala264-Ile281) and the α -7 helix (Ser285-Ser295) (Fig. 1).

In 2004, Wiesmann et al. [11] had identified new inhibitors targeted at the allosteric site of PTP1B. This provided a major impetus towards identification of non-catalytic PTP1B inhibitors with higher specificity and lesser side effects. The allosteric site is located ~20 Å away from the active site enclosed by the α -helical triad consisting of α -3 helix (Glu186-Glu200), α -6 helix (Ala264-Ile281) and the α -7 helix (Ser285-Ser295). Reports have shown the importance of α -7 helix and its substantial role in the activation and allosteric regulation of PTP1B [12]. Due to the unavailability of crystal structures of PTP1B with the WPD loop open-inactive form along with the allosteric α -7 helix, the α -7 helix has been homology modelled to PDBID-1T49 from the PTP1B closed-active structure PDBID-1SUG [13]. Earlier studies in our lab have identified six natural compounds: chlorogenic acid (CGA) and cichoric acid (CHA) isolated from *Cichorium intybus* [14, 15], Aloe emodin glycoside (AEG) from *Cassia fistula* [16], 3 β -taraxerol from *Mangifera indica* [17], (3 β)-stigmast-5-en-3-ol from *Adhatoda vasica* [18] and methyl lignocerate from *Costus pictus* [19] to exhibit antidiabetic and antiadipogenic activity by maintaining the glucose and lipid homeostasis. The structures of these six compounds

Fig. 1 Structure of PTP1B



are represented in Fig. 2. PTP1B is a strategic target involved in type 2 diabetes, aided by insulin resistance associated obesity risks [20, 21]. Our studies have shown CGA, CHA, 3BT and AEG to significantly exhibit PTP1B inhibition in biochemical assays, but their mode of binding and mechanism remained unclear [14–16]. Further investigation towards understanding the molecular inhibition mechanism showed CGA and CHA to exhibit a non-competitive inhibition of active fragment of PTP1B (1–321) in the co-incubation assay and an allosteric binding in computational studies [22].

Interestingly, using biochemical studies, a non-competitive inhibitor MSI-1436 has been identified which showed an alteration in the affinity and efficacy depending on the presence of a disordered C-terminal domain in PTP1B. MSI-1436 showed less affinity binding near α -7 helix for the PTP1B (1–321) fragment and a high-affinity binding near the disordered α -9' helix for the PTP1B (1–405) fragment [23]. Since active site-based drug discovery have failed to identify promising drugs with PTP1B specificity at clinical trials and molecular design studies with the unstructured disordered C-terminal domain (300–393) were not practically feasible, studies have strategically focused on identifying potent inhibitors binding near allosteric α -7 helix similar to those allosteric inhibitors reported by Wiesmann et al. using the structurally available PTP1B (1–299) active fragment [24–26]. Therefore, the current

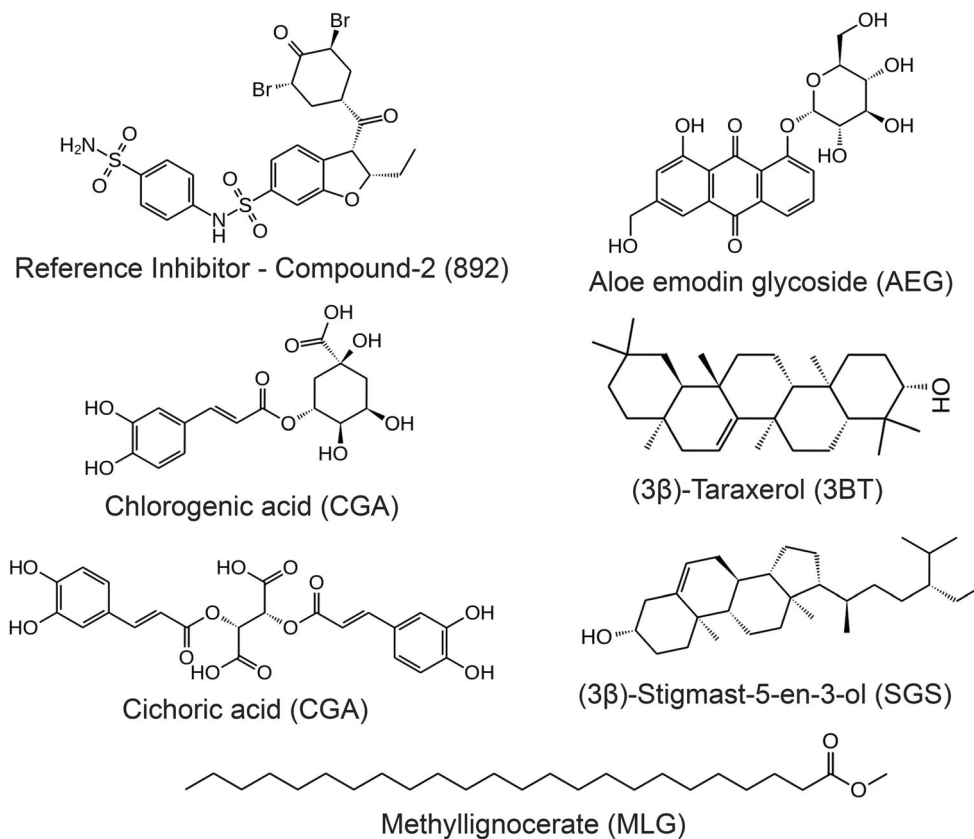
study evaluates the above mentioned six natural compounds for their allosteric inhibition ability towards PTP1B and understand its mechanism of action using computational methods.

Materials and methods

Molecular docking of PTP1B

The receptor protein structure of PTP1B was obtained from Protein Data Bank (PDBID-1T49) as an open/inactive form with truncated α -7 helix bound with compound-2 (ID 892) (IUPAC name 3-(3,5-dibromo-4-hydroxybenzoyl)-2-ethyl-benzofuran-6-sulfonic acid (4-sulfamoylphenyl)-amide) as an allosteric inhibitor [11] and optimised for rigid docking using AutoDock Tools (ADT) 1.5.6 [27]. The structure of substrate pTyr (ID PTR) O-phosphotyrosine (IUPAC name (2S)-2-amino-3-(4-phosphonoxy phenyl) propanoic acid) bound inside the active site was obtained from 1PTY (closed, active) and used for active site docking analysis [28]. The protein structure from PDBID-1SUG (closed, active form) is used for α -7 helix modelling and conformational change analysis [29].

Fig. 2 Structure of the reference inhibitor and the six bioactive natural products used in the study



The 3D coordinates of all the six plant product molecules, viz. CGA (chlorogenic acid) (IUPAC name: (1S,3R,4R,5R)-3-[(E)-3-(3,4-dihydroxyphenyl)prop-2-enoyl]oxy-1,4,5-trihydroxycyclohexane-1-carboxylic acid), CHA (cichoric acid) (IUPAC name: (2R,3R)-2,3-bis[[(E)-3-(3,4-dihydroxyphenyl)prop-2-enoyl]oxy]butanedioic acid), AEG (Aloe emodin glycoside) also known as Aloe-emodin-8-O-glycoside (IUPAC name: 1-hydroxy-3-(hydroxymethyl)-8-[3,4,5-trihydroxy-6(hydroxyl methyl)oxan-2-yl]oxyanthracene-9,10-dione), 3BT-3 β -taraxerol also known as taraxerol (IUPAC name: (3S,4aR,6aR,6aS,8aR,12aR,14aR,14bR)-4,4,6a,6a,8a,11,11,14b-octamethyl-1,2,3,4a,5,6,8,9,10,12,12a,13,14,14a-tetradecahydropicen-3-ol), SGS-(3 β)-stigmast-5-en-3-ol also known as beta-sitosterol (IUPAC name: (3S,8S,9S,10R,13R,14S,17R)-17-[(2R,5R)-5-ethyl-6-methylheptan-2-yl]-10,13-dimethyl-2,3,4,7,8,9,11,12,14,15,16,17-dodecahydro-1H-cyclopenta[a]phenanthren-3-ol), and MLG (methyl lignocerate) (IUPAC name: methyl tetracosanoate), were drawn and obtained in PDB format from the PRODRG2 server and energy minimized for 1000 steps using UCSF Chimera [30].

Molecular docking of the pTyr substrate was done in a grid box of 42, 42, 42 with a grid spacing of 0.375 Å centered on the reference substrate pTyr (PTR) at the catalytic active of PTP1B enclosed by PTP and WPD loop in open conformation with modelled α -7 helix using AutoDock v 4.2 with maximum number of active torsions allowed [27]. These parameters for active site docking were optimized by repeated docking of pTyr substrate with PTP1B to possibly get the best conformation of pTyr with the reported H-bond interactions. The best conformation with least binding energy and better interacting residues was selected. Since the other ligands are structurally bigger, molecular docking for the natural compounds were performed individually in the same place centered on the pTyr substrate with a grid box of 50, 50, 50 and a grid spacing of 0.375 Å at the active site of PTP1B.

Subsequently, the parameters for allosteric site docking were obtained by repeated docking of compound-2 (ligand 892 in 1T49) with PTP1B to possibly get the best conformation of compound-2 with the reported interactions. Molecular docking of the natural compounds with the PTP1B structure was performed individually in a grid box of 52, 52, 52 and a grid spacing of 0.375 Å centered on the position of reference inhibitor compound-2 (892) at the allosteric site of PTP1B enclosed by α -3, α -6 and α -7 helices using AutoDock v 4.2 with maximum number of active torsions allowed [27]. Each of the docking analysis was allowed to select 10 best conformations from a population of 150 individuals using the Lamarckian genetic algorithm (SA + GA) [31]. The hydrogen bond predictions were calculated within a maximum distance of 3.0 Å.

Modelling of allosteric α -7 helix to PTP1B

The α -7 helix enclosing the allosteric site of PTP1B along with α -3 and α -7 helices plays a significant role in the inhibition of the protein. But there is no crystallographic solved PTP1B structures in the open form of the WPD loop along with the α -7 helix in Protein Data Bank. So, we have modelled the allosteric α -7 helix to 1T49 (open-inactive form) for the protein and all the protein-ligand complexes and investigated the role of the α -7 helix in the allosteric inhibition of PTP1B [22, 24–26]. The modelling of the α -7 helix to PTP1B (native, open form) was performed by homology modelling with 1SUG (active, closed form) using MODELER 9v7 [32].

Molecular dynamics simulations of PTP1B

Molecular dynamics simulations of PTP1B protein (native) in comparison with PTP1B-pTyr, PTP1B-892 and the allosteric PTP1B-Ligand complexes were performed.

A total of ten simulations were performed and are represented as follows:

1. PTP1B-native protein (PTP1B protein alone without any ligand bound)
2. PTP1B-pTyr (PTP1B protein bound with pTyr substrate at the active site)
3. PTP1B-892 (PTP1B protein bound with compound-2 (892) at the allosteric site)
4. PTP1B-pTyr-892 (PTP1B protein bound with pTyr substrate at the active site and co-complexed with compound-2(892) at the allosteric site)
5. PTP1B-CGA (PTP1B protein bound with chlorogenic acid at the allosteric site)
6. PTP1B-CHA (PTP1B protein bound with cichoric acid at the allosteric site)
7. PTP1B-AEG (PTP1B protein bound with Aloe emodin glycoside at the allosteric site)
8. PTP1B-3BT (PTP1B protein bound with 3 β -taraxerol at the allosteric site)
9. PTP1B-SGS (PTP1B protein bound with (3 β)-stigmast-5-en-3-ol at the allosteric site)
10. PTP1B-MLG (PTP1B protein bound with methyl lignocerate at the allosteric site)

All the simulations were performed in a default force field GROMOS43a1 with a water box of 1.2 nm from the protein at pH 7.0 and temperature 300 K using the GROMACS 4.0.5 package [33, 34] installed in the GARUDA Cluster, CDAC, India. The topology files necessary for the simulation were calculated and obtained

using PRODRG [35]. Initially, protonation states were added to the protein residues at a pH 7.0, and the protein-ligand complexes were simulated with explicit water model in a water box of 1.2 nm from the surface of the protein. The system was neutralized with counterions, and energy minimization was performed using steepest descent algorithm for 3000 steps with allowed maximum force of 1000 KJ/mol/nm. Equilibration dynamics was performed by restraining the position of heavy atoms (protein, ligand), and the solvent molecules with counterions were allowed to move for 500 ps under NVT conditions. Finally, 100 ns of production molecular dynamics run was performed. The electrostatic interactions were calculated by the particle mesh Ewald (PME) algorithm, with an interpolation order of 4 and a grid spacing of 0.12 nm. All simulations were run under periodic boundary conditions under NVT ensemble with group scheme applied using PME algorithm in Berendsen's coupling algorithm for keeping the temperature (300 K) and the pressure (1 bar) constant along with periodic boundary conditions applied. The SHAKE algorithm was applied to fix all bonds containing hydrogen atoms with a tolerance of 10–5 Å. The time step for the simulations was 2 fs, and the coordinates were stored every 2 ps which were applied during the simulation for a timescale of 100 ns. The van der Waals (vdw) forces were treated using a cut-off of 12 Å. The analysis of trajectories was performed using GROMACS 4.0.5 package [33, 34]. Intramolecular H-bond existences were extracted and analysed using readHBmap python script, and finally, all the 2D plots were generated using GRACE [36].

PCA analysis was performed on each MD trajectories for all simulations. The snapshots saved for every 2 ps were utilised to construct a covariance matrix. Based on the diagonalization of this covariance matrix, the corresponding principal components, eigenvalues and eigenvectors were generated for each simulation. Among the several PCs generated, the first two eigenvectors covered more than 50% of the maximum variance along with more than 60% of cumulative contribution to the overall fluctuations. Hence, the PCA was performed along the first two eigenvectors to study the collective motions of the significant regions of PTP1B during each simulation.

The binding energy calculation for each protein-ligand complex simulations was done by MM-PBSA approach using the *g_mmpbsa* tool [37] with GROMACS trajectories. The binding free energy of the protein with ligand in solvent was expressed as

$$\Delta G_{\text{binding}} = G_{\text{complex}} - (G_{\text{protein}} + G_{\text{ligand}}) \quad (1)$$

where G_{complex} is the total free energy of the protein-ligand complex and G_{protein} and G_{ligand} are total free energies of the isolated protein and ligand in solvent, respectively. The free energy for each individual entity can be given by

$$G_x = \langle E_{\text{MM}} \rangle - TS + \langle G_{\text{solvation}} \rangle \quad (2)$$

where x is the protein or ligand or protein-ligand complex. $\langle E_{\text{MM}} \rangle$ is the average molecular mechanics potential energy in a vacuum. TS refers to the entropic contribution to the free energy in a vacuum where T and S denote the temperature and entropy, respectively. The term $\langle G_{\text{solvation}} \rangle$ is the free energy of solvation. The vacuum potential energy, E_{MM} , includes the energy of both bonded as well as non-bonded interactions and is calculated based on the molecular mechanics (MM) force-field parameters.

$$E_{\text{MM}} = E_{\text{bonded}} + (E_{\text{vdW}} + E_{\text{elec}}) \quad (3)$$

where E_{bonded} is bonded interactions consisting of bond, angle, dihedral and improper interactions. The non-bonded interactions ($E_{\text{non-bonded}}$) include both electrostatic (E_{elec}) and van der Waals (E_{vdW}) interactions respectively. Here in the single trajectory approach, the conformation of protein and ligand in the bound and unbound forms are assumed to be identical, and the ΔE_{bonded} is always taken as zero. The solvation free energy is expressed as the following two terms:

$$G_{\text{solvation}} = G_{\text{polar}} + G_{\text{non-polar}} \quad (4)$$

where G_{polar} and $G_{\text{non-polar}}$ are the electrostatic and non-electrostatic contributions to the solvation free energy, respectively. The energy component calculation methodologies defined and implemented in the *g_mmpbsa* tool have been used for the relative binding energy calculation and analysis.

Rescoring using Glide docking

All the ligands were individually subjected to extra precision Glide docking by selecting pTyr as the reference ligand centered at the active site of PTP1B after increasing ligand length to 20 Å to accommodate structurally bigger natural product ligands using Glide and the submodules of Schrodinger-2018 Software Suite [38–40]. Further, the allosteric protein-ligand complexes obtained from docking using AutoDock before and after α -7 helix modelling, and the complexes at 0 ns and after 100 ns of molecular dynamics simulations were rescored using Glide and the submodules of Schrodinger-2018 Software Suite [38–40]. Each of the protein-ligand complexes were individually rescored using refined extra

precision scoring of one-step docking at the allosteric site groove with compound-2 (892) as the reference inhibitor for scoring the allosteric binding ligands. All the molecules were comparatively analysed by Glide extra precision docking score, and the interaction residues at its site were generated and analysed using Maestro.

Results and discussion

Molecular docking analysis

Initially, molecular docking analysis of pTyr substrate at the active site was performed to understand the interactions of active site residues of PTP1B with its substrate O-phosphotyrosine-pTyr (PTR). Results show H-bond interactions of the substrate with the reported active site residues at Cys215, Ser216, Lys120, Arg221 and Gln262 with a least binding energy of -5.38 kcal/mol (Supplementary Fig. 1). Similarly, docking analysis of the reference allosteric inhibitor compound-2 (892) performed at the allosteric site of PTP1B showed 2 stable H-bond interactions with Asn-193, Glu276 and Pi-Pi stacking with Phe280 and Phe196 in 1T49 (Supplementary Fig. 2).

Molecular docking of the selected natural compounds performed at both the active and allosteric sites of PTP1B was analysed based on their least energy conformations and H-bond interactions with the surrounding residues. Comparative docking analysis of the reference inhibitor compound-2 (892) and the ligands performed at

the active site of PTP1B showed the ligands to exhibit significantly lesser score and less number of H-bonds compared with their docking score at the allosteric site, respectively (Table 1). This could be due to the fact that the ligands were structurally unsuitable to sufficiently fit deep into the active site pocket compared with the allosteric site (Supplementary Fig. 3). The best docking conformations of each ligands represented in Table 1 are individually shown with their significant allosteric H-bond interactions to PTP1B (Supplementary Figs. 4a to 4f). Therefore, based on docking scores, orientation of the ligands observed in these docking analyses, and previous reports of non-competitive binding in the biochemical assays [22], we postulate that binding of these natural product compounds at the allosteric site was observed to be more favourable. Therefore, further modelling and molecular dynamics simulation analysis were performed for the docked complexes at the allosteric site.

Homology modelling of alpha-7 helix at the allosteric site of PTP1B

Since the role of α -7 helix in the overall activation of the protein dynamics of PTP1B has been well established, the allosteric α -7 helix was modelled to the C-terminal of PTP1B by homology modelling before MD simulations [12, 22, 24–26, 41]. All the modelled structures were evaluated using Ramachandran plots (data not shown) which showed increased amino acid occupancies

Table 1 AutoDock docking score of all ligands compared for active site docking and allosteric site docking with PTP1B along with their H-bond interaction residues

Ligands	Active site docking		Allosteric site docking	
	Docking score (kcal/mol)	H-bond interaction residues	Docking score (kcal/mol)	H-bond interaction residues
Active site substrate pTyr (PTR)	-5.38	Cys215, Ser216, Lys120, Arg221 Gln262	–	–
Allosteric inhibitor compound-2 (892)	-8.58	Gly183, Ser216, Gln266	-10.54	Asn193, Glu276, Pi-Pi stacking with Phe280 and Phe196
Chlorogenic acid (CGA)	-3.53	Gly183, Lys120, Gln262	-5.85	Asn193, Ala189, Glu200, 2 bonds with Lys197
Cichoric acid (CHA)	-4.27	Ser216, Ala217, Gln262	-5.74	Asn193, Phe280, Ile281, 2 bonds with Glu276
Aloe emodin glycoside (AEG)	-3.92	2 bonds with Pro180, Lys120	-6.43	Asn193, Ala189, 2 bonds with Ile281, Pi-Pi stacking with Phe280
3 β -Taraxerol (3BT)	-7.01	Asp48	-9.23	Ser187
(3 β)-Stigmast-5-en-3-ol (SGS)	-6.45	No H-bond	-7.81	No H-bond
Methyl lignocerate (MLG)	-1.53	Lys120	-4.72	Arg199

at the favourable regions confirming the validity of the modelled structures.

Molecular dynamics simulation analysis

Molecular dynamics simulations for a timescale of 100 ns were performed separately for native protein(a) in comparison with the docked complexes such as protein with pTyr substrate (b) at the active site, protein with reference inhibitor (c) at the allosteric site and protein with each bioactive ligand (e–i) at the allosteric site. Additionally, the docked conformations of PTP1B-PTR at the active site and the PTP1B-compound-2 at the allosteric site were superimposed and merged as PTP1B-pTyr-892 co-complex (d) (Supplementary Fig. 5) towards probing the allosteric modulation of the inhibitor when substrate is bound at the active site during molecular dynamics.

Protein stability and fluctuation analysis

Molecular dynamics simulations of native PTP1B and the protein-ligand complexes (a to i) with the modelled allosteric α -7 helix were performed for a timescale of 100 ns each and comparatively analysed for dynamical changes in their molecular interactions.

RMSD analysis shows the PTP1B-native protein to fluctuate till 45 ns and then attain steady state dynamics at 0.27 nm with very slight fluctuation till 100 ns. The protein-ligand complexes tend to follow different levels of RMSD fluctuation based on their ligand interaction profiles and attain stability (Fig. 3a). Figure 3b shows the RMSF analysis of the C- α atoms of each amino acid residues of PTP1B during 100-ns simulations in the presence of different ligands in comparison with PTP1B-native protein(a). Substantial fluctuations were observed at the WPD loop region for the PTP1B-pTyr(b) signifying dynamical changes due to binding of substrate at the active site along with its associated fluctuations at PTP loop, S loop, α -3 helix and the allosteric α -7 helix. However, no significant levels of fluctuations were observed at the WPD loop for the protein-inhibitor complexes.

The dynamical variation of the WPD loop when substrate is bound at the active site PTP1B-pTyr(b) was further studied by evaluating the minimum distance deviation between the C- α atoms of Asp181 of the WPD loop and Ser216 of the PTP loop enclosing the active site. Figure 3c shows a decrease in the minimum distance profile between the active site amino acids from 1.1 nm to less than 0.8 nm at 30 ns which was maintained at 0.7 nm till 100 ns for the PTP1B-native protein(a). This suggests that the PTP1B protein is inclining towards auto-activation by changing its conformation from open, inactive state to closed active state in the absence of ligands. In the presence of active site substrate PTP1B-pTyr(b), the fluctuation was observed to be around 0.8 nm

maintaining the stable interaction with the pTyr substrate at the active state. This conformational change of WPD loop correlates with earlier studies [41–45]. This restrained WPD loop distance fluctuation was observed to be higher for the other protein-ligand complexes except for PTP1B-SGS(i) and PTP1B-MLG(j) which were observed to show a decrease after 85 ns and 90 ns, respectively.

Total energy analysis of the protein and protein-ligand complex simulations was observed to be significantly low for PTP1B-native protein(a) (– 899,000 KJ/mol) and PTP1B-pTyr(b) (– 901,000 KJ/mol). However, the total energies of the PTP1B-inhibitor complexes were greater than – 850,000 KJ/mol as shown in Supplementary Fig. 6. Similarly, analysis of the potential energy profile of the PTP1B-native protein(a) and PTP1B-pTyr(b) showed less energy of – 1,100,000 KJ/mol and – 1,130,000 KJ/mol, respectively. The potential energies of the PTP1B-inhibitor complexes were observed to be greater than – 1,042,000 KJ/mol (Supplementary Fig. 7). This increase in energy values could be due to the size of the allosteric bound ligands and their binding energy compared with the small and readily binding substrate molecule pTyr. Analysis of the radius of gyration profile shows the compactness of the PTP1B protein to be maintained at 1.9 nm with minimal fluctuations in the native protein similar to all the protein-ligand simulations, confirming that there was no unusual protein uncoiling or irregular protein unfolding during the simulation of 100 ns (Supplementary Fig. 8).

Hydrogen bond interaction and allosteric inflection analysis

Average protein-ligand distance analysis was performed to understand the binding stability and orientation of the respective ligands with PTP1B. Results show that ligands waver in the respective binding cleft to interact with the protein by maintaining a constant overall distance. Among them, the pTyr substrate was observed to maintain a closer distance of around 1.2 nm and 1.4 nm at the active site in both PTP1B-pTyr(b) and PTP1B-pTyr-892(d) simulations, respectively. But the allosteric ligands were observed to be slightly higher around 2 nm and maintained their respective distances with the protein (Supplementary Fig. 9). This suggests that the pTyr substrate remains deep and buried in active site pocket compared with the ligands at the allosteric site.

Previous studies have reported that the H-bond interaction of the allosteric inhibitor compound-2 varies and dynamically changes between the α -helical triad at the allosteric site [11–13]. Therefore, variations in H-bonded interaction of each ligand with the protein were analysed by calculating the number of H-bonds formed in the complex. Results show the substrate pTyr in PTP1B-pTyr(b) to form 7–9 H-bonds compared with the pTyr in PTP1B-pTyr-892(d) which was observed to form 6–7 H-bonds, probably due to the allosteric constraint

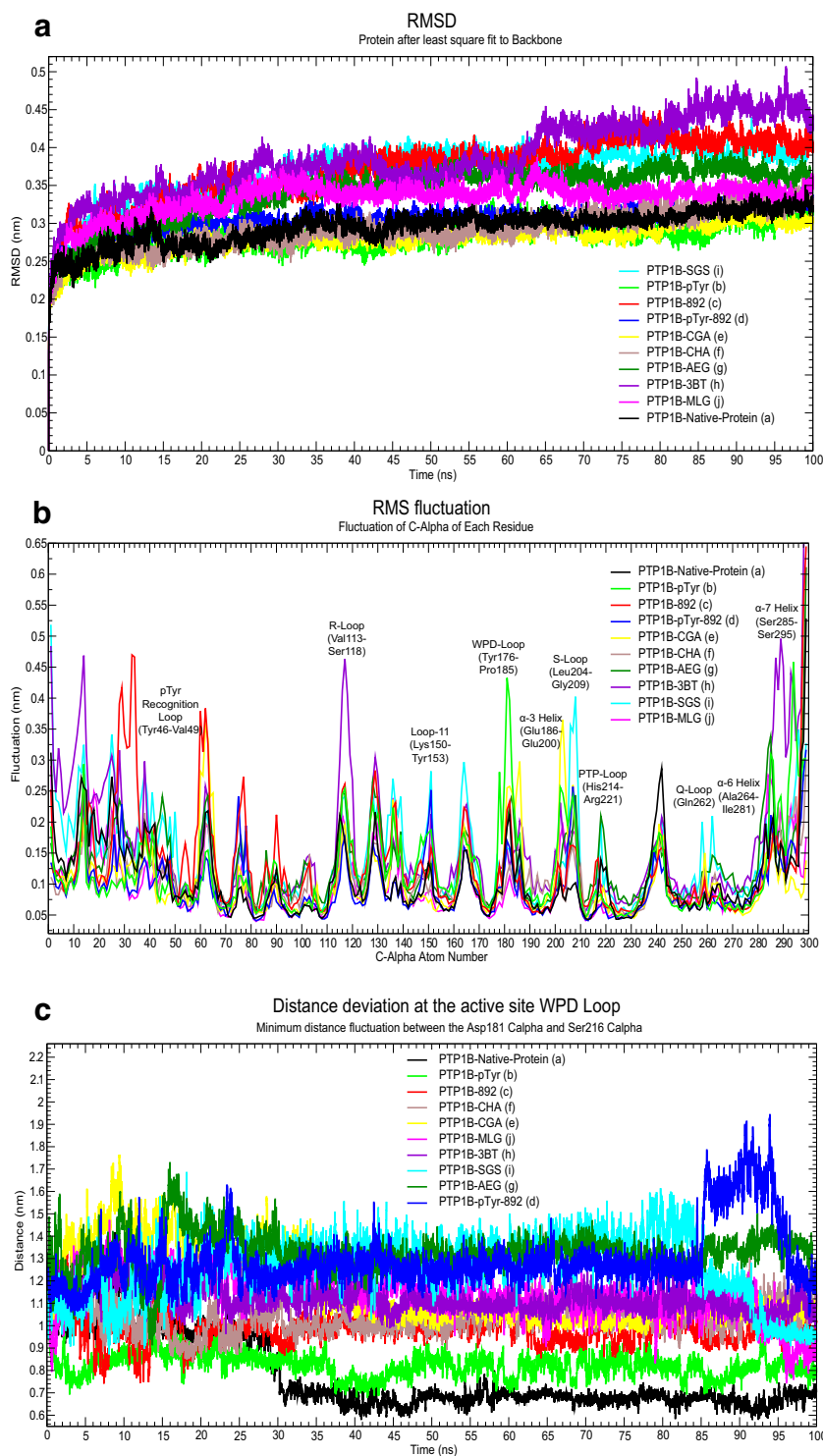


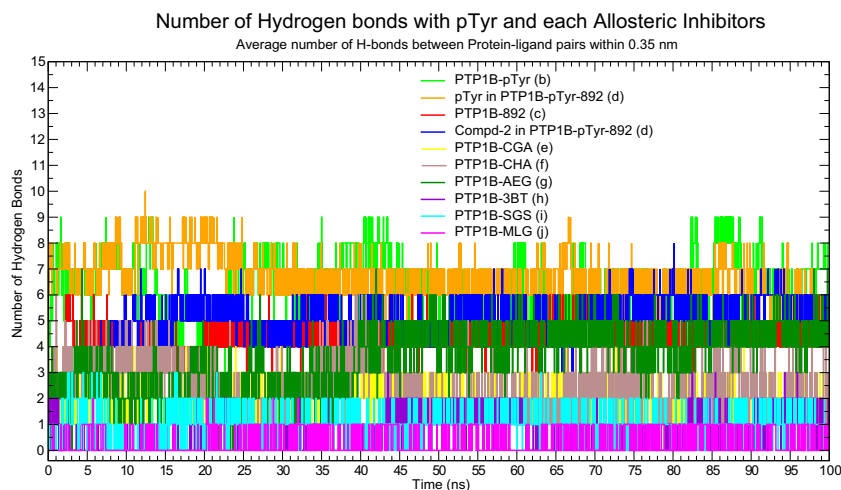
Fig. 3 **a** RMSD profile of native PTP1B, protein and the protein-ligand complexes with the modelled α -7 helix during MD simulations for 100 ns. **b** RMSF profile of PTP1B with modelled α -7 helix, native protein in comparison with protein-ligand complexes during the MD

simulations of 100 ns. **c** Minimum distance deviation profile between Asp181 of WPD loop and Ser216 of PTP loop at the active site in PTP1B with modelled α -7 helix represented as native protein in comparison with protein-ligand complexes during the MD simulations of 100 ns

caused by compound-2 (892). Also, AEG, CGA, CHA and 3BT were observed to form 3–5 H-bonds, while SGS and MLG showed less than 2 H-bond interaction (Fig. 4).

Previous MD simulations have elucidated the significant role of α -7 helix and its underlying interactions responsible for the conformational stability of PTP1B [12, 41, 46]. Hence,

Fig. 4 Number of H-bond profile between the ligands and PTP1B in the simulations with modelled α -7 helix represented for pTyr substrate (active site) in comparison with allosteric ligands during the timescale of 100 ns



the allosteric modulation caused by these ligands was probed by measuring the minimum distance profile between Asn193 of α -3 helix and Leu292 of α -7 helix. Results show that for the PTP1B-native protein(a) and PTP1B-pTyr(b) complex, the α -3 helix and α -7 helix are maintained at a distance below 0.7 nm, leading to closer interactions (Fig. 5). However, in the protein-allosteric ligand complexes except for PTP1B-SGS(i), the distance stayed above 0.8 nm. This outward movement of the α -7 helix caused by the bound ligands could be due to changes in interactions of the allosteric helical triad.

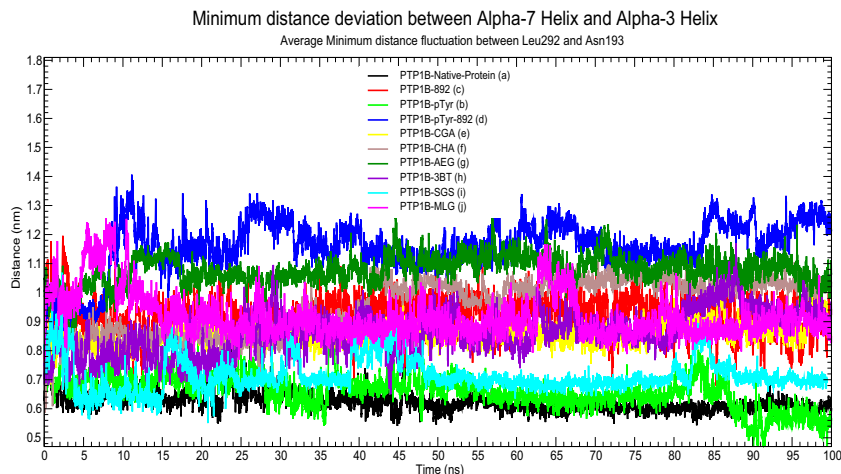
To further investigate the movement of the α -3 and α -7 allosteric helices, relative distances between their axes were measured by considering them as helical bundles. Results show the distance between the α -7 helix and α -3 helix bundle axes to be maintained between 0.55 and 0.6 nm in the PTP1B-native protein(a) and PTP1B-pTyr(b) in comparison with the dynamics of other protein-ligand complexes (Supplementary Fig. 10). Tilting angle analysis of α -7 helix with the α -3 helix showed a correlated increase of 25–40° for the protein-inhibitor complexes, whereas for the PTP1B-native protein(a) and PTP1B-pTyr(b) complexes, the fluctuation was observed to be around 18 and 22°, respectively (Supplementary

Fig. 11). These changes imply that the α -7 helix changes its orientation and moves away from the α -3 helix due to interactions with the allosteric inhibitors. These movements correlate with previous reports on the interactions between α -3 and α -7 helices involved in allosteric inhibition mechanism of PTP1B [26, 41, 47].

Analysis of the distance between the α -7 helix and α -6 helix bundle axis showed the distance to be 0.74 nm for the PTP1B-native protein(a) and PTP1B-pTyr(b) complex, whereas a slight decrease of around 0.68 nm was observed for the allosteric inhibitor complexes of CGA, CHA, AEG and 3BT. However, PTP1B-SGS(i) and PTP1B-MLG(j) complexes showed distances greater than 0.8 (Supplementary Fig. 12).

Correspondingly, the interhelical tilting angle analysis between α -7 helix and α -6 helix showed the angle to be around 38° between the helices for the PTP1B-native protein(a) and PTP1B-pTyr(b) complexes. The interhelical tilting angle among the other complexes was observed to be decreased (Supplementary Fig. 13). These interhelical analyses show that the allosteric inhibitors CGA, CHA, AEG, 3BT and compound-2 mediate the repulsive movement of α -7 helix

Fig. 5 Minimum distance profile between α -3 helix (Asn193) and α -7 helix (Leu292) in PTP1B simulations with modelled α -7 helix represented as native protein in comparison with protein-ligand complexes during the timescale of 100 ns



aided by the pulling of α -6 helix closer around 0.65 nm, thereby, restraining its interaction distance with the α -3 helix around 0.8 nm.

H-bonding interaction between the ligands and binding sites

Although all the ligands were observed to maintain an overall constant distance with the protein, the H-bond interactions between the protein and ligand appeared to be changing dynamically during simulations. Allosteric inhibition of compound-2 was reported to be mediated by bonded and non-bonded interactions with residues of allosteric helices such as Ala189, Leu192, Asn193, Phe196, Lys197, Glu200, Glu276, Lys279, Phe280, Ser285, Val287, Gln288 and Trp291 [11, 13, 41]. Hence, H-bonding pattern for each ligand was inspected individually by analysing the mean distance between H-bond donor and acceptor atom pairs in correlation with the possible number of H-bonds.

Analysis of the distance of H-bonding atom pairs between pTyr substrate in the active site during the PTP1B-pTyr(b) simulations show that each of three O atoms of phosphate to form alternating H-bonds with the active site PTP loop residues Cys215, Ser216, Ala217, Gly218, Ala219, Arg221 and Gln262 with OH atom by maintaining a distance less than 0.35 nm during simulation. Intermittent H-bond interactions alternatively formed between PTR:O and PTR:OXT groups with the surrounding residues Lys120:HZ1, Tyr46:HH and Asp181:NH2 were observed by their fluctuation below 0.5 nm. These H-bond interaction changes correlate with the fluctuation of WPD loop in Supplementary Fig. 14a suggesting that pTyr maintains the closed-active form of WPD loop by managing the interactions on both sides of the active site (PTP loop and WPD loop) [43, 44].

Supplementary Fig. 14b shows the interaction analysis of the co-complex with pTyr at the active site of PTP1B when compound-2 is bound at the allosteric site. pTyr was observed to maintain a distance below 0.35 nm between the three O atoms of the phosphate and the PTP loop residues Ser216, Ala217, Gly218, Gly219, Gly220 and Arg221. Ser222 was observed to form new alternating bond between the O1P and O3P atoms. But the distances between PTR:H2 and PTR:OXT groups with the surrounding residues Lys120:HZ1, Tyr46:OH and Asp181:OD2 were observed to be increasing above 0.5 nm indicating an outward movement of the WPD loop from the pTyr towards an inactive-open form as shown in Supplementary Fig. 14b. Therefore, although the pTyr stays in the active site close to the PTP loop, it is unable to hold and interact with the WPD loop due to the restrained modulation of allosteric α -helices by compound-2.

H-bonding analysis of compound-2 and the allosteric site residues in the PTP1B-892(c) shows compound-2 to maintain a distance below 0.35 nm from the residues Glu276, Lys279, Asp284, Ser285, Val287, Ser296 and Glu4 (Supplementary

Fig. 14c). But the distance between Asn193 and 892:OD19 appeared to be increased and maintained above 0.4 nm leading to a loss of the H-bond, allowing compound-2 to orient itself to form better H-bonding interaction with the modelled α -7 helix.

Supplementary Fig. 14d shows the variation of H-bonds between compound-2 and residues in the allosteric site due to active site pTyr substrate in the PTP1B-pTyr-892(d) co-complex simulations. The ligand compound-2 forms interchanging interactions by maintaining a distance below 0.35 nm between the atoms of compound-2 and the residues Glu276, Asp284, Gln288, Gln290, Trp291 and alternating distance of 0.2 nm–0.4 nm with Asp289, Ser295 and Asn193–892:OD19. However, the distance between Asn193–892:OD20 and Lys279–892:O3 appeared to be increased and maintained above 0.4 nm, leading to a loss of H-bonds. This could be due to the Compound-2 forming alternating H-bonding with the Helical triad, leading to inhibition of the PTP1B-pTyr-892(d) co-complex, by restraining the WPD loop in an inactive form as shown in Fig. 3c.

Among the ligands assessed in the study, CGA was observed to form fluctuating interactions with residues Asn193, Lys197, Lys292, Gln288-CGA:OAA and Gln288-CGA:HAD by maintaining a distance of 0.2–0.4 nm between the atom pairs (Supplementary Fig. 14e). CHA in PTP1B-CHA(f) was observed to form highly fluctuating interaction with residues Asn193:OD1, Phe196:O, Gln288:HE22, Lys292, Gln288-CHA:OAA and Gln288-CHA:HAD by maintaining a distance of 0.2 nm–0.4 nm between the atom pairs, while there is a loss of H-bonds with Asn193:HD21, Lys197, Arg199 and Trp291 due to an increase in distance above 0.5 nm (Supplementary Fig. 14f). AEG in PTP1B-AEG(g) was observed to form highly fluctuating interactions with residues Gly277, Leu232, Asp236 Trp291, Gln288 and Asn193 due to reduction in a distance of 0.2–0.4 nm between the atom pairs (Supplementary Fig. 14g). However, a loss in H-bond interactions with Lys197, Glu200 and Phe280 was observed after 45 ns. This distance change suggests that AEG interacts with the helical triad to enter deep into the cavity between the α -3 and α -6 helices by limiting the interaction of α -7 helix for better protein inhibition. 3BT in PTP1B-3BT(h) was observed to form variable interactions with the residues of Ser187, Ala189, Pro188 and Glu276 by an alternating distance of 0.2–0.6 nm between the atom pairs leading to a loss of H-bond interactions (Supplementary Fig. 14h). However, for Asn193:OD1 and Asn193:HD21, there is reduction in distance of 0.3 nm after 80 ns enabling formation of H-bonds.

SGS in PTP1B-SGS(i) was observed to form alternating interactions with residues Lys197, Lys292 and His296 by their fluctuating distance of 0.2–0.5 nm between the atom pairs leading to a loss of H-bonds (Supplementary Fig. 14i). The loss of H-bonds with residues Asn193:OD1 and Asn193:HD21 was

observed due to an increase in distance above 0.5 nm after 15–20 ns. Although SGS appears to orient itself towards better interaction with the helical triad, the fluctuation is not effective towards protein inhibition as shown in Fig. 3c. Similarly, MLG in PTP1B-MLG(j) forms highly discontinuous interaction with residues Ser286, Gly283 and Lys239 with a large distance of 0.2–0.7 nm between the atom pairs having transient H-bonds (Supplementary Fig. 14j). A loss in H-bond interaction with residue Asp284 due to an increase in distance above 0.75 nm after 10 ns was observed. Thus, MLG is ineffective in allosteric interaction for protein inhibition coinciding with the WPD loop fluctuations in Fig. 3c.

Relative binding energy analysis by MM-PBSA

To study the non-bonded interactions and individual energy components associated with bonded interactions, the relative binding free energy ΔG_{bind} analyses were performed by the MM-PBSA method. Figure 6 represents the relative binding energy ΔG_{bind} fluctuation for each of the ligands throughout 100 ns of simulations. For pTyr, the substrate at the active site, the binding energy was observed to fluctuate around -35 KJ/mol in (b, d) after 45 ns of stabilisation. The B.E. (Binding Energy) for CHA (f) was observed to be higher than 450 KJ/mol compared with the other allosteric inhibitors 892 (c, d), CGA (e) and AEG (g). 3BT (h) and SGS (i) showed binding energies less than -200 KJ/mol and -150 KJ/mol, respectively.

Table 2 shows the comparison of components involved in the relative binding energy for each ligand. Results show decreased non-polar solvation free energies (ΔE_{nonpol}) for all the ligands. For pTyr and the reference allosteric inhibitor (compound-2/892), the binding energies are observed to be majorly contributed by the balancing values of electrostatic interaction energy (ΔE_{ele}) and polar solvation free energy (ΔE_{pol}). However, for the other allosteric inhibitors, the binding energies appear to be mainly contributed by moderate values of

van der Waals interaction energy (ΔE_{vdw}) and polar solvation free energy (ΔE_{pol}), with the exception of CHA with a higher B.E. of around 390 KJ/mol and MLG with a large B.E. of 4000 KJ/mol (data plot could not be shown in Fig. 6 due to the extreme range). Though the binding energy of CHA was observed to be 390 KJ/mol, changes in the H-bond interactions and restrained allosteric helical movements substantiate that CHA was able to alternate allosteric interactions mediating moderate inhibition of PTP1B (Supplementary Fig. 10–13, 22a–b). The binding affinity for MLG was observed to be high at 4000 KJ/mol and failed to exhibit effective modulation of allosteric helices due to its weak interactions with the helices (Supplementary Fig. 26a–b).

Essential dynamics analysis

To understand the dynamical motion of significant amino acid regions contributing to major collective motions during the molecular dynamics of all native PTP1B and PTP1B-ligand complexes, principal component analysis (essential dynamics analysis) was performed. Figure 7a shows the plot of maximum variance of the top eigenvector index values derived from the diagonalization of the covariance matrix of the atomic fluctuations that showed high fluctuation of PTP1B-ligand complexes for the top 15 eigenvectors in comparison with the native PTP1B dynamics. Also, Fig. 7b represents the cumulative contribution profile for the top 15 eigenvectors. The results confirm that the first and second eigenvectors exhibit maximum variation and account for 70–80% of principal fluctuation in the overall dynamics compared with the remaining eigenvectors studied.

Hence, the major fluctuating residues contributing to the collective motions were studied along the first and second eigenvectors. RMSF analysis of PTP1B residues along the first eigenvector depicted in Supplementary Fig. 15 showed significantly high fluctuations of around 5.0 Å at the active site—WPD loop (Thr177-Pro185),

Fig. 6 Relative binding energy profile of each ligand plotted separately for all protein-ligand complexes during the timescale of 100-ns simulations

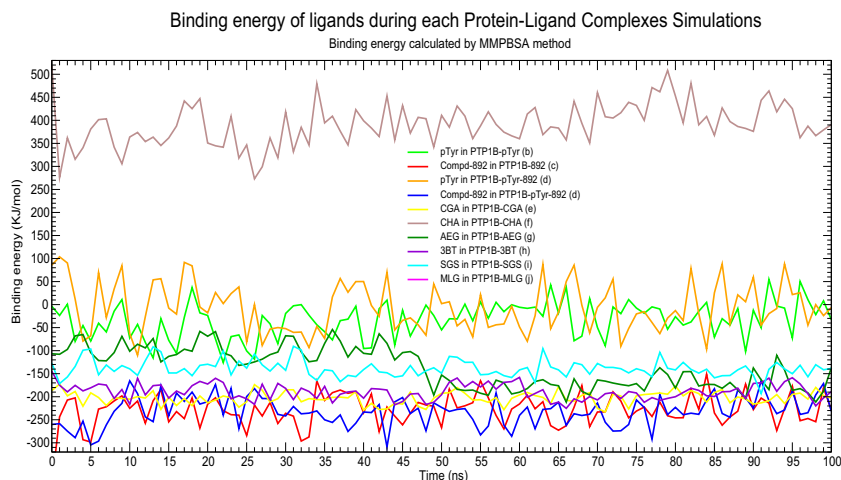


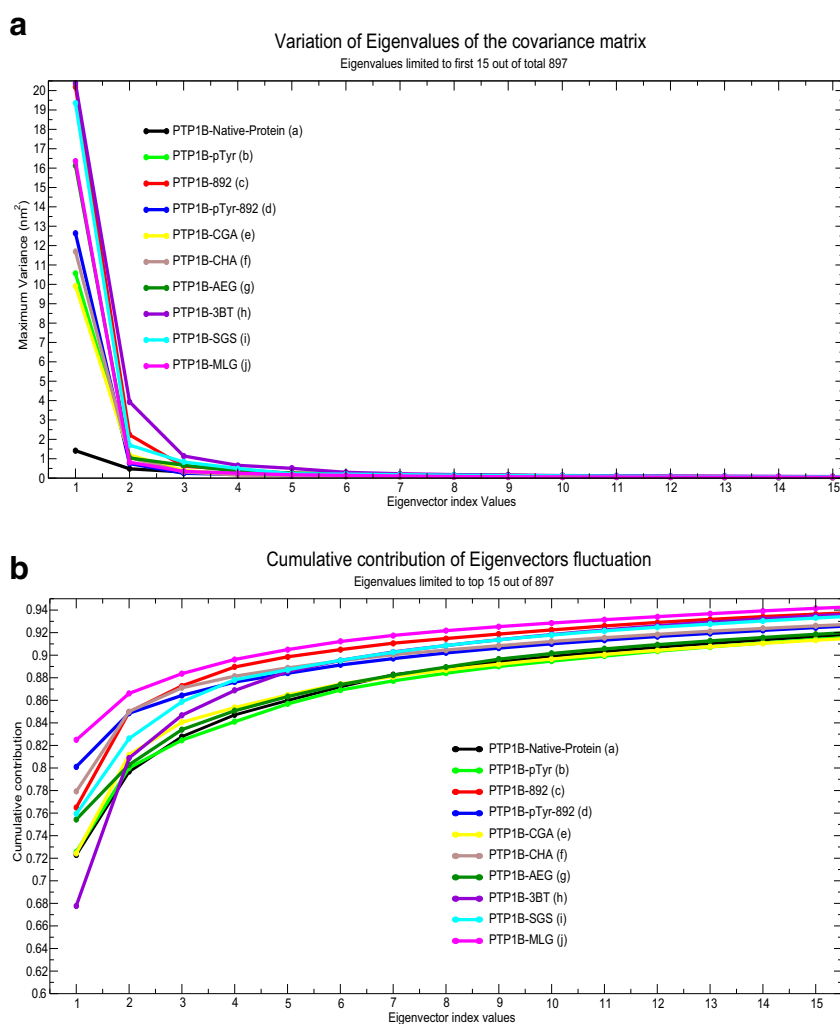
Table 2 Binding energy and individual energy component values of ligands in each protein-ligand complexes calculated by MM-PBSA methods

Protein-ligand complex simulations	Energy components—average values in kJ/mol				
	Interaction energies		Solvation free energies		Avg. relative binding energy ΔG_{bind}
	ΔE_{vdw}	ΔE_{ele}	ΔE_{pol}	ΔE_{nonpol}	
PTP1B-pTyr(b)	-133.640	-448.313	561.469	-12.290	-32.774
PTP1B-892(c)	-225.027	-728.138	745.681	-21.284	-228.768
pTyr in PTP1B-pTyr-892(d)	-120.099	-417.996	571.861	-10.405	-36.639
Compound-2 in PTP1B-pTyr-892(d)	-231.217	-761.614	783.021	-21.883	-231.694
PTP1B-CGA(e)	-267.365	-8.271	89.180	-16.231	-202.687
PTP1B-CHA(f)	-197.991	303.637	301.833	-16.720	390.759
PTP1B-AEG(g)	-201.274	-39.999	171.157	-17.069	-187.185
PTP1B-3BT(h)	-211.774	-8.086	49.137	-18.286	-189.010
PTP1B-SGS(i)	-200.285	-4.255	83.553	-17.612	-138.599
PTP1B-MLG(j)	4110.381	-60.168	149.644	-18.763	4181.094

PTP loop (His214-Arg 221) and R loop (Val113-Ser118) for both native PTP1B and PTP1B-ligand complexes. However, the PTP1B-ligand complexes were also

observed to show higher fluctuations of more than 5.0 Å along S loop (Ser201-Gly209) and alpha-7-helix (Val287-Ser295).

Fig. 7 **a** Variance profile of the top 15 eigenvalues of the covariance matrix represented for protein and protein-ligand complexes during the timescale of 100-ns simulations. **b** Cumulative contribution profile of the top 15 eigenvalues of the covariance matrix represented for protein and protein-ligand complexes during the timescale of 100 ns simulations



These fluctuations reveal the inhibitory modulation caused by the PTP1B-ligand complexes is at the active site, through protein structural conformation changes from the allosteric site. Also, fluctuations of these amino acids were observed to correlate with the active site distance deviation profile shown in Fig. 3c. RMSF analysis of PTP1B residues along the second eigenvector showed decreased fluctuations at the active site—WPD loop (Thr177-Pro185), S loop (Ser201-Gly209) and R loop (Val113-Ser118) for native PTP1B and around 0.2-nm fluctuation for the PTP1B-ligand complexes (Supplementary Fig. 16). Taken together, these residues appear to principally contribute to the overall dynamics in comparison with the other eigenvector dynamics. Supplementary Fig. 17 shows the 2D projection of eigenvector-1 towards eigenvector-2 and the tendency of trajectory movement of PTP1B in the PTP1B-native protein(a) compared with PTP1B-pTyr(b) substrate complex and the other PTP1B allosteric inhibitors. Results show PTP1B-native protein(a) and PTP1B-pTyr(b) to follow similar dynamical movement due to their activation being enabled by the closing of WPD loop and substrate interactions. The allosteric inhibitor complexes exhibited different dynamics based on their allosteric modulation.

Validation by Glide score analysis

Glide extra precision docking score of the ligands performed at active site compared with the allosteric site score showed each ligand to exhibit significantly lesser score and less number of H-bonds compared with their score at the allosteric site (Supplementary Table 1). Superimposed ligand structures at the active site of PTP1B (Supplementary Fig. 18) reveal that the variations in docking score were due to the unsuccessful fitting of these natural compounds in the active site pocket paralleled to their effective and substantial binding at the

allosteric site. These results correlate with the variations in the AutoDock docking score.

For further confirmation, all the docked complexes obtained from docking of the ligands at the allosteric site without α -7 helix using AutoDock were rescored using the Glide module of Schrodinger. Since the docking of pTyr substrate was done at the active site, the Glide docking score remained the same both in the presence and absence of the allosteric α -7 helix (Table 3). Glide docking results for the allosteric ligands showed that the predicted conformations were similar based on their docking score and bonded interactions in the absence of the allosteric α -7 helix (Table 3). But the Glide score of these allosteric ligand complexes after homology modelling of the allosteric α -7 helix changed based on their refined interaction between the residues of modelled α -7 helix at the allosteric site.

Finally, Glide rescoring analysis by extra precision docking was done for all the ligand complexes before (at 0 ns) and after (at 100 ns) molecular dynamics simulations. These Glide scores show the ligands to dynamically adjust and orient at their binding site for better and potent interactions during the 100-ns simulations (Table 3).

The interactions of pTyr at the active site for PTP1B-pTyr(b) shown in Supplementary Fig. 19a–19b shows how the interactions change from the open/inactive WPD loop at 0 ns to the closed/active WPD loop-based interaction with Asp-181 to Pi-Pi stacking with Phe182 and Pi-cation interaction with Arg221 along with increased H-bonded and non-bonded interactions at the active site at 100 ns. These interactions significantly correlate with the previous reported interactions of pTyr substrate with the active site residues in PTP loop and WPD loop [45].

compound-2 (892) at the allosteric site of PTP1B-892(c) shown in Supplementary Fig. 20a–20b show the interactions to change after 100 ns towards better Pi-Pi

Table 3 Docking score of ligands in each protein-ligand complexes scored by Glide module of Schrodinger 2018 Inc.

Protein-ligand complex simulations	Glide extra precision docking score (kcal/mol)			
	Without modelled α -7 helix	With modelled α -7 helix	With α -7 helix, MDS complexes	
			0 ns	100 ns
pTyr in PTP1B-pTyr(b) Substrate (active site)	-9.012	-9.012	-6.929	-8.819
Compd-2 in PTP1B-892(c)	-8.217	-10.731	-10.791	-9.461
Ref. allosteric inhibitor				
CGA in PTP1B-CGA(e)	-5.706	-8.136	-7.995	-8.221
CHA in PTP1B-CHA(f)	-5.864	-8.321	-7.207	-9.083
AEG in PTP1B-AEG(g)	-7.163	-8.906	-9.725	-10.190
3BT in PTP1B-3BT(h)	-6.512	-8.054	-8.324	-9.900
SGS in PTP1B-SGS(i)	-6.440	-7.131	-7.076	-6.709
MLG in PTP1B-MLG(j)	-4.931	-6.331	-6.661	-4.170

stacking with Phe280 and Trp291 with increased H-bonded and non-bonded interactions with the crucial allosteric α -7 helix [11, 13].

Similarly, analysis of the interactions of other allosteric inhibitors showed better coordination and optimised interactions after molecular dynamics except for SGS and MLG. Supplementary Fig. 21a–21b show CGA to form 2 H-bonded and more hydrophobic interactions with α -7 helix after 100 ns than at 0 ns in PTP1B-CGA(e) in correlation with its Glide score, whereas CHA in PTP1B-CHA(f) formed 2 H-bonds and 2 salt-bridge interactions at 100 ns interacting between α -3 and α -7 helices each as shown in Supplementary Fig. 22a–22b [22].

AEG in PTP1B-AEG(g) at 100 ns was observed to form more stable Pi-Pi stacking with Phe196 and Phe280 and 5 H-bonded interactions between α -3 and α -6 helices than at 0 ns getting deeper at the allosteric pocket by pushing the α -7 helix outwards as shown in Supplementary Fig. 23a–23b. However, 3BT in PTP1B-3BT(h) was unable to form H-bonds due to its single hydroxyl group, although it maintained hydrophobic and polar interactions during dynamics at 0 ns and 100 ns as shown in Supplementary Fig. 24a–24b.

SGS in PTP1B-SGS(i) stayed in the allosteric groove and finally formed one H-bond with His296 during 100 ns and had very less hydrophobic interactions as shown in Supplementary Fig. 25a–25b. But MLG in PTP1B-MLG(j) that had one H-bond with Ser286 of α -7 helix at 0 ns was observed to move outwards from the allosteric site forming new H-bond with Lys239 outside the allosteric helical triad at 100 ns from the allosteric helices as shown in Supplementary Fig. 26a–26b.

Allosteric inhibition pathway analysis

Recent reports on the mechanism of allosteric inhibition of PTP1B indicates that the transition between the open and closed conformation of WPD loop is induced by its interaction with the adjacent α -3 helix and Loop11 through the conformational rearrangement of α -7 helix [46, 47]. Hence, in this study, we analysed the changes in protein structure linked to the allosteric inhibition by probing the dynamical intramolecular H-bond occupancy interaction between the key domain regions during the stabilised timescale of 40 to 100 ns. The H-bonding residues pairs that have the highest possible occupancy between each group have been tabulated under the specific column in Supplementary Table 2.

The internal H-bond interaction between PTP loop and WPD loop showed that for PTP1B-native protein(a) and PTP1B-pTyr(b), the residue Arg221 of PTP loop interacts with the residues Asp181/Phe182 of WPD loop with more than \sim 50% H-bond occupancy, due to less distance of active conformation of WPD loop closing over the active site. However, this interaction was reduced for the other

simulations with allosteric inhibitors. Correspondingly, intra-H-bond interaction between R loop and WPD loop shows that the interaction of Lys116 forms \sim 40% H-bond interaction with Asp181 in PTP1B-native-protein(a), and Val113 forms \sim 40% H-bond alternating with Tyr176 and Thr177 in PTP1B-pTyr(b). These alternating bonds indicate that the WPD loop is staying favourably in closed conformation through its interaction with R loop surrounding the active site. These H-bond interactions of WPD loop with PTP loop and R loop were considerably less for other simulations with the allosteric bound inhibitors (c–j). These analyses correlate with the distance deviation profile of WPD loop in the active site shown in Fig. 3c. The H-bond interaction between Loop11- α -3 helix show the residues Tyr152/Tyr153 to alternate with Ser190 and Asn193 with more than \sim 60% occupancy for PTP1B-native protein(a). For PTP1B-pTyr(b) simulations, the H-bond interactions between WPD loop α -3 helix and Tyr176 with Ser190 are few with less than \sim 20% occupancy, thereby indicating the activated interaction for the closed WPD loop conformation.

Contrary to these fluctuations, simulations c–h with allosteric site inhibitors showed the interaction with Loop11 α -3 helix to be lesser than 20% H-bond occupancy, and interactions between WPD Loop α -3 helix to be more than \sim 60% H-bond occupancy. These results correlate with the previous reports of Liu et al. on the crucial role of the Tyr176-Ser190 interaction in the outward movement of WPD loop and conservation of the catalytic loop in open-inactive conformation. But for the simulations (i–j), the WPD loop α -3 helix interactions were lesser than 50% with corresponding lesser interactions between Loop11 α -3 helix indicating that the inhibitors SGS and MLG were less efficient at the allosteric site. Further, to study the coordination involved in the outward movement of the α -7 helix, H-bond interactions between the α -6- α -7 helices and α -7- α -3 helices pairs were analysed. Results show the H-bond occupancy between the α -6 and α -7 helices to be more than \sim 40% in the simulations with allosteric ligand complexes (c–g) with an interrelated decrease in the H-bond occupancy less than \sim 20% for α -7 helix- α -3 helix interaction. These facts coincide with the distance profile and interhelical angle results (Supplementary Fig. 10–13) confirming that the allosteric ligands enable the outward movement α -7 helix being pulled by the α -6 helix interactions aided by disturbing the α -7 helix bonding with α -3 helix. However, for the simulations (i–j) with SGS and MLG, H-bond interactions between α -6 helix and α -7 helix were less with relatively higher interaction occupancy between α -7 helix and α -3 helix denoting their inability in the allosteric modulation (Supplementary Table 2). This allosteric pathway analysis clearly demonstrates that the mechanism of allosteric inhibition has been intermediated by adaptable intramolecular H-bond interactions between

the Loop11, α -3 Helix, WPD Loop and α -7 Helix. Also, the dynamical variations in the intramolecular H-bonds between the characteristic regions taking place in the presence of the six ligand molecules determine that AEG, 3BT, CHA and CGA have relatively better ability in moderating allosteric inhibition compared with SGS and MLG.

Conclusions

There have been various molecular dynamics studies to understand the molecular interactions of PTP1B with different inhibitors both at the active and allosteric sites along with their interaction with protein residues. This study shows the potential activity of six structurally different natural compounds CGA, CHA, AEG, 3BT, SGS and MLG to interact at the allosteric site of PTP1B and their efficiency in accomplishing non-catalytic inhibition through structural dynamics. Comparative docking studies at the active and allosteric site of PTP1B showed these compounds to exhibit favourable binding at the allosteric site. Further, docking studies predicted the most favourable least energy conformations with significant H-bond interactions similar to the reference allosteric inhibitor compound-2(892) for the six compounds. Molecular dynamics simulations performed for 100 ns with the modelled α -7 helix for each protein-ligand complexes in comparison with the reference inhibitor compound-2 revealed the prominent interactions of each compound and their conformational rearrangement mechanism involved in the allosteric inhibition of PTP1B.

The activational conformational change of WPD loop inclining towards closed-active form after 35 ns during simulation for PTP1B-native protein(a) exhibited auto-activation dynamics of the PTP1B protein in the absence of ligands. Similarly, PTP1B-pTyr(b) dynamics represented the pTyr substrate mediated interaction enabling the activation of WPD loop closing over the active site. These dynamical observations were confirmed by the WPD loop with PTP loop/R loop distance profiles and interaction profiles showing that the dynamical closing of WPD loop was facilitated mainly through structural interactions of Loop11 with α -3 helix along with the allosteric bonded interactions of α -3 helix with α -7 helix. However, during simulations with reference inhibitor compound-2, PTP1B-892(c) and the substrate inhibitor bound co-complex PTP1B-pTyr-892(d), these bonded interactions of WPD loop with α -3 Helix were altered by the allosteric ligand maintaining the WPD loop in its open-inactive state. PCA and H-bonding analysis shows the hindrance of WPD activation to be due to the allosteric pathway-mediated interaction of Tyr176 with Ser190 disrupting the interaction between Loop11, α -3 helix and α -7 helix. These interactions substantiate the outward movement of the allosteric α -7 helix responsible for the allosteric inhibitions. This outward movement of allosteric α -7 helix attained by interaction changes

between α -3 helix and α -6 helix, validated by the distance deviation and interhelical angle analysis, correlates with previous studies on allosteric mechanism.

Characteristically, the novel co-complex simulation PTP1B-pTyr-892(d) showed the allosteric pathway-mediated interactions to be prominent and effectively strong towards sustaining WPD inactivation by the reference inhibitor compound-2 in spite of the pTyr substrate-bound interaction at the active site. Finally, comparison of the allosteric proficiency of these six compounds with compound-2 during dynamics showed PTP1B-AEG(g) to exhibit better H-bonded interactions with α -3 helix and α -7 helix and also intermediated better restriction of WPD closing through stable Tyr176-Ser190 interactions aided by the outward pulling with α -6 helix- α -7 helix interactions. PTP1B-3BT(h) showed steady interactions at the allosteric site with better interaction of Tyr176-Ser190 along with the α -6 helix- α -7 helix. PTP1B-CHA(f) and PTP1B-CGA(e) exhibit the next-level efficacy through better interactions at the allosteric site and WPD inactivation through the allosteric pathway. Analysis of PTP1B-SGS(i) and PTP1B-MLG(j) showed these compounds to exhibit lesser allosteric interactions and are unable to mediate strong WPD loop hindrance due to variable interactions between Loop11 with α -3 helix and α -7 helix with α -3 helix. MM-PBSA binding energy analysis of the compounds correlated with the movement of allosteric site residues, indicating that MLG showed out of range unfavourable interactions.

Glide score validation of the final structures based on binding and site interaction confirms the inhibition potency of each compound at the allosteric site stating that AEG had more interactions similar to compound-2 (892). Hence, this study probes the possibility and the effectiveness of allosteric modulation of six different natural compounds towards PTP1B inhibition using molecular dynamics and their underlying protein structural modifications involved for inhibition. These results enumerate the importance of α -7 helix of PTP1B along with its coordination with WPD loop, Loop11, α -3 helix and α -6 helix. The changes caused in intramolecular bonding and interaction profiles due to these compounds would provide better insight towards understanding the allosteric modulation mechanism, enabling design of new, efficient allosteric inhibitors for PTP1B.

Acknowledgements The authors thank Dr. T. Kothai and Dr. P. Gautam for their constant support and encouragement. The authors are grateful to Dr. Subrata Chattopadhyay (C-DAC) and Janaki Chintalapati (C-DAC) for providing access to computational resources of the GARUDA Cluster facility, C-DAC, Government of India, to run the Gromacs v4.0.5-MD Simulations during 2013–2015.

Funding information The authors thank the Department of Biotechnology, Govt of India for financial assistance for the HPC cluster computer for Drug Design and related commercial Schrodinger software

through the DBT-BUILDER (BT/PR12153/INF/22/200/2014), and the DBT-BTIS-DIC facility at Centre for Biotechnology, Anna University, Chennai. The author Mr. SarathKumar B sincerely thanks the Council for Scientific and Industrial Research, Govt. of India, for financial assistance as CSIR-SRF (09/468(0480)/2014-EMR-1).

Compliance with ethical standards

Conflict of interest The authors declare that they have no conflict of interest.

References

- Elchebly M, Payette P, Michaliszyn E, Cromlish W, Collins S, Loy AL, Normandin D, Cheng A, Himms-Hagen J, Chan CC, Ramachandran C, Gresser MJ, Tremblay ML, Kennedy BP (1999) Increased insulin sensitivity and obesity resistance in mice lacking the protein tyrosine phosphatase-1B gene. *Science* 283(5407):1544–1548
- Klaman LD, Boss O, Peroni OD, Kim JK, Martino JL, Zabolotny JM, Moghal N, Lubkin M, Kim YB, Sharpe AH, Stricker-Krongrad A, Shulman GI, Neel BG, Kahn BB (2000) Increased energy expenditure, decreased adiposity, and tissue-specific insulin sensitivity in protein-tyrosine phosphatase 1B-deficient mice. *Mol Cell Biol* 20(15):5479–5489
- Fauman EB, Saper MA (1996) Structure and function of the protein tyrosine phosphatases. *Trends Biochem Sci* 21(11):413–417
- Barford D, Flint AJ, Tonks NK (1994) Crystal structure of human protein tyrosine phosphatase 1B. *Science* 263(5152):1397–1404
- Zhang ZY (2001) Protein tyrosine phosphatases: prospects for therapeutics. *Curr Opin Chem Biol* 5(4):416–423
- Johnson TO, Ermolieff J, Jirousek MR (2002) Protein tyrosine phosphatase 1B inhibitors for diabetes. *Nat Rev Drug Discov* 1(9):696–709
- Kolmodin K, Aqvist J (2001) The catalytic mechanism of protein tyrosine phosphatases revisited. *FEBS Lett* 498(2–3):208–213
- Montalibet J, Skorey K, McKay D, Scapin G, Asante-Appiah E, Kennedy BP (2006) Residues distant from the active site influence protein-tyrosine phosphatase 1B inhibitor binding. *J Biol Chem* 281(8):5258–5266
- Jia Z, Barford D, Flint AJ, Tonks NK (1995) Structural basis for Phosphotyrosine peptide recognition by protein tyrosine phosphatase 1B. *Science* 268(5218):1754–1758
- Kamerlin SC, Rucker R, Boresch S (2007) Molecular dynamics study of WPD-loop flexibility in PTP1B. *Biochem Biophys Res Commun* 356(4):1011–1016
- Wiesmann C, Barr KJ, Kung J, Zhu J, Erlanson DA, Shen W, Fahr BJ, Zhong M, Taylor L, Randal M, McDowell RS, Hansen SK (2004) Allosteric inhibition of protein tyrosine phosphatase-1B. *Nat Struct Mol Biol* 11(8):730–737
- Olmez EO, Alakent B (2011) Alpha7 helix plays an important role in the conformational stability of PTP1B. *J Biomol Struct Dyn* 28(5):675–693
- Bharatham K, Bharatham N, Kwon YJ, Lee KW (2008) Molecular dynamics simulation study of PTP1B with allosteric inhibitor and its application in receptor based pharmacophore modeling. *J Comput Aided Mol Des* 22(12):925–933
- Muthusamy VS, Anand S, Sangeetha KN, Sujatha S, Arun B, Lakshmi BS (2008) Tannins present in *Cichorium intybus* enhance glucose uptake and inhibit adipogenesis in 3T3-L1 adipocytes through PTP1B inhibition. *Chem Biol Interact* 174:69–78
- Muthusamy VS, Saravanababu C, Ramanathan M, Bharathi Raja R, Sudhagar S, Anand S, Lakshmi BS (2010) Inhibition of protein tyrosine phosphatase 1B and regulation of insulin signalling markers by caffeoyl derivatives of chicory (*Cichorium intybus*) salad leaves. *Br J Nutr* 104(6):813–823
- Anand S, Muthusamy VS, Sujatha S, Sangeetha KN, Bharathi Raja R, Sudhagar S, Poornima Devi N, Lakshmi BS (2010) Aloe emodin glycosides stimulates glucose transport and glycogen storage through PI3K dependent mechanism in L6 myotubes and inhibits adipocyte differentiation in 3T3L1 adipocytes. *FEBS Lett* 584(14):3170–3178
- Sangeetha KN, Sujatha S, Muthusamy VS, Anand S, Nithya N, Velmurugan D, Balakrishnan A, Lakshmi BS (2010) 3beta-taraxerol of *Mangifera indica*, a PI3K dependent dual activator of glucose transport and glycogen synthesis in 3T3-L1 adipocytes. *Biochim Biophys Acta* 1800(3):359–366
- Sujatha S, Anand S, Sangeetha KN, Shilpa K, Lakshmi J, Balakrishnan A, Lakshmi BS (2010) Biological evaluation of (3β)-STIGMAST-5-EN-3-OL as potent anti-diabetic agent in regulating glucose transport using in vitro model. *Int J Diabetes Mellitus* 2(2):101–109
- Shilpa K, Sangeetha KN, Muthusamy VS, Sujatha S, Lakshmi BS (2009) Probing key targets in insulin signaling and adipogenesis using a methanolic extract of *Costus pictus* and its bioactive molecule, methyl tetracosanoate. *Biotechnol Lett* 31(12):1837–1841
- Popov D (2011) Novel protein tyrosine phosphatase 1B inhibitors: interaction requirements for improved intracellular efficacy in type 2 diabetes mellitus and obesity control. *Biochem Biophys Res Commun* 410(3):377–381
- Panzhinskiy E, Ren J, Nair S (2013) Pharmacological inhibition of protein tyrosine phosphatase 1B: a promising strategy for the treatment of obesity and type 2 diabetes mellitus. *Curr Med Chem* 20(21):2609–2625
- Sarath Kumar B, Goswami N, Selvaraj S, Muthusamy VS, Lakshmi BS (2012) Molecular dynamics approach to probe the allosteric inhibition of PTP1B by chlorogenic and cichoric acid. *J Chem Inf Model* 52(8):2004–2012
- Krishnan N, Koveal D, Miller DH, Xue B, Akshinthala SD, Kragelj J, Jensen MR, Gauss CM, Page R, Blackledge M, Muthuswamy SK, Peti W, Tonks NK (2014) Targeting the disordered C terminus of PTP1B with an allosteric inhibitor. *Nat Chem Biol* 10(7):558–566
- Jin T, Yu H, Huang XF (2016) Selective binding modes and allosteric inhibitory effects of lupane triterpenes on protein tyrosine phosphatase 1B. *Sci Rep* 6:20766-1–20766-14
- Zargari F, Lotfi M, Shahraki O, Nikfarjam Z, Shahraki J (2018) Flavonoids as potent allosteric inhibitors of protein tyrosine phosphatase 1B: molecular dynamics simulation and free energy calculation. *J Biomol Struct Dyn* 36(15):4126–4142
- Shinde RN, Kumar GS, Eqbal S, Sobhia ME (2018) Screening and identification of potential PTP1B allosteric inhibitors using in silico and in vitro approaches. *PLoS One* 13(6):e0199020
- Morris GM, Huey R, Lindstrom W, Sanner MF, Belew RK, Goodsell DS, Olson AJ (2009) Autodock4 and AutoDockTools4: automated docking with selective receptor flexibility. *J Comput Chem* 16:2785–2791
- Puius YA, Zhao Y, Sullivan M, Lawrence DS, Almo SC, Zhang ZY (1997) Identification of a second aryl phosphate-binding site in protein-tyrosine phosphatase 1B: a paradigm for inhibitor design. *Proc Natl Acad Sci U S A* 94(25):13420–13425
- Pedersen AK, Gü PG, Møller KB, Iversen LF, Kastrup JS (2004) Water-molecule network and active-site flexibility of apo protein tyrosine phosphatase 1B. *Acta Crystallogr D Biol Crystallogr* 60(Pt 9):1527–1534
- Pettersen EF, Goddard TD, Huang CC, Couch GS, Greenblatt DM, Meng EC, Ferrin TE (2004) UCSF Chimera—a visualization system for exploratory research and analysis. *J Comput Chem* 25(13):1605–1612

31. Morris GM, Goodsell DS, Halliday RS, Huey R, Hart WE, Belew RK, Olson AJ (1998) Automated docking using a Lamarckian genetic algorithm and an empirical binding free energy function. *J Comput Chem* 19(14):1639–1662
32. Webb B, Sali A (2016) Comparative protein structure modeling using MODELLER. *Curr Protoc Bioinformatics* 54:5.6.1–5.6.37
33. Van Der Spoel D, Lindahl E, Hess B, Groenhof G, Mark AE, Berendsen HJ (2005) GROMACS: fast, flexible and free. *J Comput Chem* 26(16):1701–1718
34. Hess B, Kutzner C, Van Der Spoel D, Lindahl E (2008) GROMACS 4: algorithms for highly efficient, load-balanced, and scalable molecular simulation. *J Chem Theory Comput* 4(3):435–447
35. Schüttelkopf AW, Van Aalten DM (2004) PRODRG - a tool for high-throughput crystallography of protein-ligand complexes. *Acta Crystallogr D Biol Crystallogr* 60(Pt 8):1355–1363
36. Turner PJ. XMGRACE, version 5. Center for Coastal and Land-Margin Research, Oregon Graduate Institute of Science and Technology, Beaverton, Oregon; 2005. <http://plasma-gate.weizmann.ac.il/Grace/>
37. Kumari R, Kumar R, Lynn A (2014) g_mmpbsa-a GROMACS tool for high-throughput MM-PBSA calculations. *J Chem Inf Model* 54(7):1951–1962
38. Halgren TA, Murphy RB, Friesner RA, Beard HS, Frye LL, Pollard WT, Banks JL (2004) Glide: a new approach for rapid, accurate docking and scoring. 2. Enrichment factors in database screening. *J Med Chem* 47:1750–1759
39. Friesner RA, Murphy RB, Repasky MP, Frye LL, Greenwood JR, Halgren TA, Sanschagrin PC, Mainz DT (2006) Extra precision glide: docking and scoring incorporating a model of hydrophobic enclosure for protein-ligand complexes. *J Med Chem* 49(21):6177–6196
40. Sastry GM, Adzhigirey M, Day T, Annabhimoju R, Sherman W (2013) Protein and ligand preparation: parameters, protocols, and influence on virtual screening enrichments. *J Comput Aided Mol Des* 27(3):221–234
41. Shinde RN, Sobhia ME (2013) Binding and discerning interactions of PTP1B allosteric inhibitors: novel insights from molecular dynamics simulations. *J Mol Graph Model* 45:98–110
42. Kumar R, Shinde RN, Ajay D, Sobhia ME (2010) Probing interaction requirements in PTP1B inhibitors: a comparative molecular dynamics study. *J Chem Inf Model* 50(6):1147–1158
43. Peters GH, Frimurer TM, Andersen JN, Olsen OH (1999) Molecular dynamics simulations of protein-tyrosine phosphatase 1B. I ligand-induced changes in protein motions. *Biophys J* 77(1):505–515
44. Peters GH, Frimurer TM, Andersen JN, Olsen OH (2000) Molecular dynamics simulations of protein-tyrosine phosphatase 1B. II Substrate-enzyme interactions and dynamics. *Biophys J* 78(5):2191–2200
45. Kamerlin SC, Rucker R, Boresch S (2006) A targeted molecular dynamics study of WPD loop movement in PTP1B. *Biochem Biophys Res Commun* 345(3):1161–1166
46. Cui W, Geng LL, Liang DS, Hou TJ, Ji MJ (2013) Unraveling the allosteric inhibition mechanism of PTP1B by free energy calculation based on umbrella sampling. *J Chem Inf Model* 53(5):1157–1167
47. Li S, Zhang J, Lu S, Huang W, Geng L, Shen Q, Zhang J (2014) The mechanism of allosteric inhibition of protein tyrosine phosphatase 1B. *PLoS One* 9(5):e97668

Publisher's note Springer Nature remains neutral with regard to jurisdictional claims in published maps and institutional affiliations.